# 1 Interrelationships between cellulase activity and

# 2 cellulose particle morphology

- 3 Johan P Olsen<sup>1</sup>, Bryon S. Donohoe<sup>2</sup>, Kim Borch<sup>3</sup>, Peter Westh<sup>1</sup> and Michael G. Resch<sup>4\*</sup>
- <sup>4</sup> Research unit for Functional Biomaterials, Department of Science, Systems and Models,
- 5 Roskilde University, DK-4000 Roskilde, Denmark
- 6 <sup>2</sup>Biosciences Center, National Renewable Energy Laboratory, Golden, CO
- Novozymes A/S, Krogshøjvej 36, DK-2880 Bagsværd, Denmark
- 8 4National Bioenergy Center, National Renewable Energy Laboratory, Golden, CO
- \*Corresponding author: Michael G. Resch, <u>michael.resch@nrel.gov</u>, (303) 384-7854

## 11 Acknowledgements

- 12 This work was supported by the Danish Council for Strategic Research, Program
- 13 Commission on Sustainable Energy and Environment (grant # 11-116772 to P.W.),
- Augustinus Foundation (# 14-4639 to JO) and Oticon Foundation (# 14-3925 to JO).
- 15 BSD and MGR were supported by the DOE Office of Energy Efficiency & Renewable
- 16 Energy (EERE), Bioenergy Technologies Office (BETO). The authors gratefully
- acknowledge associate professor Morten F. Pedersen and assistant professor Per M.
- 18 Jepsen for their assistance with statistical analyses and coulter counter measurements,
- 19 respectively.

#### Keywords

20

23

24

25

26

27

28

29

30

31

32

33

34

35

36

37

38

39

40

41

42

43

- 21 Imaging, Transmission Electron Microscopy, cellulose surface structure, cellulase,
- 22 cellobiohydrolase, endoglucanase

#### Abstract

It is well documented that the enzymatic hydrolysis of cellulose follows a reaction pattern where an initial phase of relatively high activity is followed by a gradual slowdown over the entire course of the reaction. This phenomenon is not readily explained by conventional factors like substrate depletion, product inhibition or enzyme instability. It has been suggested that the underlying reason for the loss of enzyme activity is connected to the heterogeneous structure of cellulose, but so far attempts to establish quantitative measures of such a correlation remain speculative. Here, we have carried out an extensive microscopy study of Avicel particles during extended hydrolysis with Hypocrea jecorina cellobiohydrolase 1 (CBH1) and endoglucanase 1 and 3 (EG1 and EG3) alone and in mixtures. We have used differential interference contrast microscopy (DICM) and transmission electron microscopy (TEM) to observe and quantify structural features at um and nm resolution, respectively. We implemented a semi-automatic image analysis protocol, which allowed us to analyze almost 3000 individual micrographs comprising a total of more than 300,000 particles. From this analysis we estimated the temporal development of the accessible surface area throughout the reaction. We found that the number of particles and their size as well as the surface roughness contributed to surface area, and that within the investigated degree of conversion (< 30%) this measure correlated linearly with the rate of reaction. Based on this observation we argue that cellulose structure, specifically surface area and roughness, plays a major role in the ubiquitous rate loss observed for cellulases.

### 44 Introduction

Essentially all reported experiments have shown that the enzymatic hydrolysis of
cellulose exhibits a gradual loss of activity as the reaction progresses. This behavior is
only partially explained by product inhibition, substrate depletion and physical
instability of the enzymes (Zhang and Lynd 2004), and the underlying reasons for the
ubiquitous slowdown has been the subject of much debate (Bansal et al. 2009). In the
very early stage of enzymatic hydrolysis turnover slow-down might be explained by the
processive nature of cellulases (Jalak and Väljamäe 2010; Praestgaard et al. 2011), and
some reports have indicated that other enzyme effects like inactivation, unproductive
binding or enzyme crowding might influence activity during extended hydrolysis as well
(Eriksson et al. 2002; Yang et al. 2006). Nonetheless, most recent work has concluded,
that the continued rate loss is mainly substrate dependent (Arantes and Saddler 2011;
Bansal et al. 2012; Hong et al. 2007; Jeoh et al. 2007; Luterbacher et al. 2015) even
though relationships between substrate alterations and the reduced rate of hydrolysis
remain poorly understood. Undoubtedly part of the rate decrease can be attributed to
the heterogeneous nature of cellulose; in addition to being an insoluble polymer it is a
mixture of amorphous and crystalline regions forming fibrils of various sizes depending
on the cellulose source (Payne et al. 2015). This heterogeneity has been proposed to
contribute to the observed rate loss. Thus it has often been suggested that the
amorphous parts are degraded preferentially, leaving behind crystalline regions that are
more recalcitrant towards degradation (Zhang and Lynd 2004), but reports that the
crystallinity index of cellulose is unaffected by enzymatic degradation (Hall et al. 2010),
has directed attention towards more continuous effects like changes in accessible
surface area, pore size or available reactive sites on the substrate has also been
proposed (Bansal et al. 2009; Grethlein 1985). Based on mechanistic models it has been
suggested that change in substrate surface area is an important factor for the decline in

70 hydrolysis rate (Levine et al. 2010). Hence, Bansal et al concluded that 90% of the rate 71 decline is caused by a decrease in substrate accessibility and hydrolysability – a 72 quantity the authors define as the fraction of enzyme binding sites that are available for 73 hydrolysis (Bansal et al. 2012). 74 Many studies have sought to clarify changes undergone by cellulosic substrates during 75 hydrolysis using high resolution imaging techniques like atomic force microscopy 76 (AFM), transmission or scanning electron microscopy (TEM, SEM) or fluorescence 77 microscopy. Whole pretreated biomass has a complex architecture across multiple 78 length scales, and while this architecture has been studied extensively for many 79 different substrates (Antal 1985; Ciesielski et al. 2014; Donohoe and Resch 2015), only 80 in rare cases have structural effects of enzymatic degradation of these substrates been 81 reported (Resch et al. 2014). In contrast numerous studies on enzyme induced changes 82 to the morphology of pure cellulose substrates like BMCC ribbons, Valonia fibrils and 83 Avicel have been published over the years (for an extensive review see Bubner et al. 84 2013). The general observation is that cellobiohydrolases (CBHs) – notably CBH1 – 85 target crystalline regions while endoglucanases (EGs) target amorphous regions, and 86 that the combined action of the two types of enzymes has a profoundly different effect 87 than each of them alone (Bubner et al. 2013; Payne et al. 2015). Furthermore it has been 88 found that CBHs degrades cellulose fibrils from the ends and cause narrowing and 89 sharpening of the fibril and indeed entire bundles of cellulose fibrils-while EGs have no 90 apparent spatial preference and cause general surface disruption or fibrillation (Chanzy 91 and Henrissat 1985; Chanzy et al. 1983). Some studies have found that CBH1 acts to 92 clear away sub-fibrils created by EG (Sprey and Bochem 1992) while others have 93 observed that the action of CBH1 alone caused initial fibrillation, and only after 94 extensive hydrolysis left behind thinned, sharpened and recalcitrant fractions (Chanzy 95 et al. 1983; Imai et al. 1998; Jeoh et al. 2013). These studies have focused on structural 96 changes mostly from a qualitative approach, but some attempts have been made at

acquiring quantitative measures of changes in cellulose structure observed in AFM (Bubner et al. 2012; Wang et al. 2013) and fluorescence microscopy (Luterbacher et al. 2015) to elucidate the progression over time. These studies have provided valuable insights in the continuous morphological changes invoked by cellulases on cellulose substrates. However, to make continued observation of a defined area possible, the studied substrates were functionalized to a support material or solubilized and recrystallized to obtain a smooth surface. These modifications might affect the preferences for enzyme attack or alter structural integrity of the substrate and hence influence the morphological effects of enzymatic degradation. In addition the general approach is often incompatible with (or at least complicates interpretation of) bulk biochemical measurements of substrate conversion that are required for direct comparisons of substrate structure and enzymatic activity. For these reasons it is not straightforward to draw conclusions from these studies regarding any effect substrate alterations might have on cellulase slow-down. Here, we have used differential interference contrast microscopy (DICM) and transmission electron microscopy (TEM) to determine structural changes of Avicel particles at the µm-nm scale during extended hydrolysis. Avicel was chosen primarily due to the relatively narrow and well-defined size range of the particles making them well suited for the image analysis presented here. The substrate was treated with two different endoglucanases (EG1 and EG3) and a cellobiohydrolase (CBH1) from Trichoderma reesei either alone or in mixtures. To get reliable, quantitative measures of the observed structural changes we implemented automated procedures for image analyses using the open source image processing software ImageJ. This allowed us to analyze a very large number of micrographs, which was necessary due to the heterogeneity of Avicel particles. In other words we did not attempt to identify distinct structural features in individual samples but rather to obtain quantitative ensemble average measures of structure changes analogous to what is obtained in biochemical

97

98

99

100

101

102

103

104

105

106

107

108

109

110

111

112

113

114

115

116

117

118

119

120

121

122

activity measurements. This approach, along with the microscopy study being blinded, ensured an unbiased and reliable quantification of the morphological effect of cellulase activity on unmodified Avicel and allowed us to correlate these changes to the loss of hydrolytic activity.

#### Materials and methods

#### **Cellulose digestion**

124

125

126

127

128

129

130

131

132

133

134

135

136

137

138

139

140

141

142

143

144

145

146

Unless otherwise noted, all chemicals were purchased from Sigma-Aldrich. All hydrolysis reactions were carried out in 30mM sodium acetate buffer, pH 5.0 with 2 mM CaCl<sub>2</sub> and 0.01% sodium azide. Avicel PH 101 was washed by centrifugation, once in milliQ water and twice in reaction buffer. Final dry matter concentration in the reaction mixture was 10 mg/mL (1% w/v). TrCel7A, TrCel7B and TrCel12A were heterologously expressed in Aspergillus oryzae and purified as described elsewhere (Westh et al. 2014). To ensure a substantial conversion with the simple mixtures used here the enzymes were dosed at 100 mg/g Avicel either alone or in mixtures of 5%, 25%, 50% or 80% EG to total enzyme (see Table 1). Control samples were made without added enzyme. All samples were supplemented with 10mg/g β-glucosidase (*Aspergillus niger*) and incubated at 50°C with end-over-end rotation at 10rpm. Samples were taken for activity measurements at 0, 8, 24, 48, 72, and 96 hours. A subset of each sample from 0, 8, 48 and 96 hours was stored at -20°C for imaging. Glucan conversion was determined by HPLC as previously described (Resch et al. 2014). All image processing was carried out using Fiji, a distribution of the open source image processing software ImageJ (Schindelin et al. 2012). The analyses described below were written into macros to allow automatic processing.

1	4	7
1	1	Q

	1	2	3	4	5	6	7	8	9	10	11	12
CBH1	100%	0%	0%	95%	75%	50%	20%	95%	75%	50%	20%	0%
EG1	0%	100%	0%	5%	25%	50%	80%	0%	0%	0%	0%	0%
EG3	0%	0%	100%	0%	0%	0%	0%	5%	25%	50%	80%	0%

#### Differential interference contrast microscopy:

*Microscopy:* Slurries of samples were transferred directly to a glass microscope slide and a cover slip was sealed around the edges to minimize evaporation. Images were taken with a SPOT RTKE CCD camera (Diagnostic Instruments, Sterling Heights, MI) on a Nikon C1 Plus microscope (Nikon, Tokyo, Japan) in bright field mode. All images were taken using a 60X 1.4 NA Plan Apo objective resulting in 1600 x1200 pixel images covering 195 x146  $\mu$ m (corresponding to a pixel size of 122nm).

Image processing: Representative examples of DCIM micrographs before and after processing in ImageJ are shown in Figure 2 and a step-by-step walkthrough of the processing is shown in supplementary Figure S1. Initially, the contrast was enhanced, and the 24-bit RGB image was converted to a binary mask by applying the "Yen" threshold method (Kapur et al. 1985). A shadow from uneven illumination of the samples distorted the image processing along the edges of many of the DICM micrographs. To exclude this from the analysis we removed the outermost 60 pixels along all four edges of the image. Since DICM enhances contrast many particles would appear as only a perimeter. To make particles solid we applied the "Fill Holes" command before the perimeter and area as well as the maximum and minimum Feret's diameter (longest and shortest possible distance between two parallel tangents to the particle's perimeter, here used as a measure of particle length and width, respectively) was determined for each particle using Fiji's "Analyze Particles" function.

#### Transmission electron microscopy

169

170

171

172

173

174

175

176

177

178

179

180

181

182

183

184

185

186

187

188

189

190

191

192

193

194

Microscopy: 3µl sample was drop cast onto a 200 mesh carbon coated copper grid, negatively stained with 2% uranyl acetate and rinsed with water. The grids were imaged on a FEI Tecnai G2 20 Twin 200 kV LaB6 TEM (FEI, Hilsboro, OR) with a 4 megapixel Gatan UltraScan 1000 camera (Gatan, Pleasanton, CA). All images were acquired by the same operator to ensure consistent search criteria. To avoid bias the trial was blinded i.e. the operator was unaware which sample was on any particular grid. Grids were surveyed systematically at 1500x magnification and images were acquired at 3500x magnification, resulting in a frame size of 6.1 x 6.1 μm. All particles large enough to be clearly identified at 1500x (more than  $\sim 1 \mu m \log$ ) and small enough to fit in the image frame at 3500x (less than  $\sim 6 \mu m$ ) were imaged. As evident from the results section, most often a large number of much smaller particles were included in the field of view. Approximately 80-90 images were captured for each sample. *Image processing and analysis:* Noise was minimized by the "Remove Outliers" option, which changes the value of any pixel to the median of all pixel values in a surrounding block of designated size (here, 10x10 pixel) if that pixel deviates from that median by more than a specified value (1x standard deviation). Subsequently the images were converted from grayscale to a binary mask by applying the "Triangle" threshold method (Rogers et al. 1977) and the particle perimeters and areas were measured using the "Analyze Particles" procedure. Note, however, that even though holes are subtracted from particle area they are not included in the perimeter. Consequently, in images including overlapping particles these were assessed as single large particles with holes, the perimeter being only the outer perimeter of the particle. To overcome this we implemented a macro that first measured the area and perimeter of the particles and subsequently inverted the mask so as to measure the perimeter of the holes. The resulting two data files were combined with a script in Matlab (R2013a v 8.1.0.604,

Natick, Ma, USA) to get the total perimeter and area. Thus the reported values are total perimeter and area for each image as opposed to each individual particle. A step-by-step review of the entire processing of a representative TEM micrograph can be found in the supplementary material (Figure S2). Size determination by coulter counter Samples with sufficient residual volume after microscopy (28 out of the total 36 samples) were analyzed on a Multisizer 4e coulter counter fitted with a 100µm aperture (Beckman Coulter, Brea, CA), using 5‰ NaCl (0.45μm vacuum filtered) as electrolyte. Samples were diluted 1:800 in the electrolyte solution and the particles were resuspended by repeated pipetting before 1ml was analyzed. Due to the limited amount of sample material we were unable to perform replicate measurements. **Statistics** As previously reported and detailed in the supplementary information, the size distribution of Avicel particles follows a log-normal distribution (Marshall and Sixsmith 1975) which makes the average size a poor measure of the typical particle in a given sample. For this reason we have mainly used the median values in the analysis presented below. However, in the case of DICM analysis, because each micrograph contained a large number of particles we could analyze the distribution of a given parameter within each micrograph, and use the 5 individual images of each sample as analytical replicates. All analyses of correlation were carried out using the statistical software package JMP version 10 (SAS Institute Inc., Cary, NC). In the case of median length and circularity were data appeared to be linear (see Figure 3), we used Pearson's correlation analyses to determine if any such correlation could be considered significant. For particle count, spheroid surface area and surface roughness, the data was clearly non-linear and non-

195

196

197

198

199

200

201

202

203

204

205

206

207

208

209

210

211

212

213

214

215

216

217

218

monotone. To test whether the variation in each data set was random or significantly dependent on the conversion we applied Hoeffding's independence test. As detailed in the results section we divided the data into subsets but since these data sets were relatively small with considerable variation we did not find it reasonable to assume linearity (as implicitly done with Pearson's). For this reason we used the Spearman's rank analysis to test for correlation in these cases, although it should be noted that a similar outcome was found with Pearson's correlation analysis (not shown).

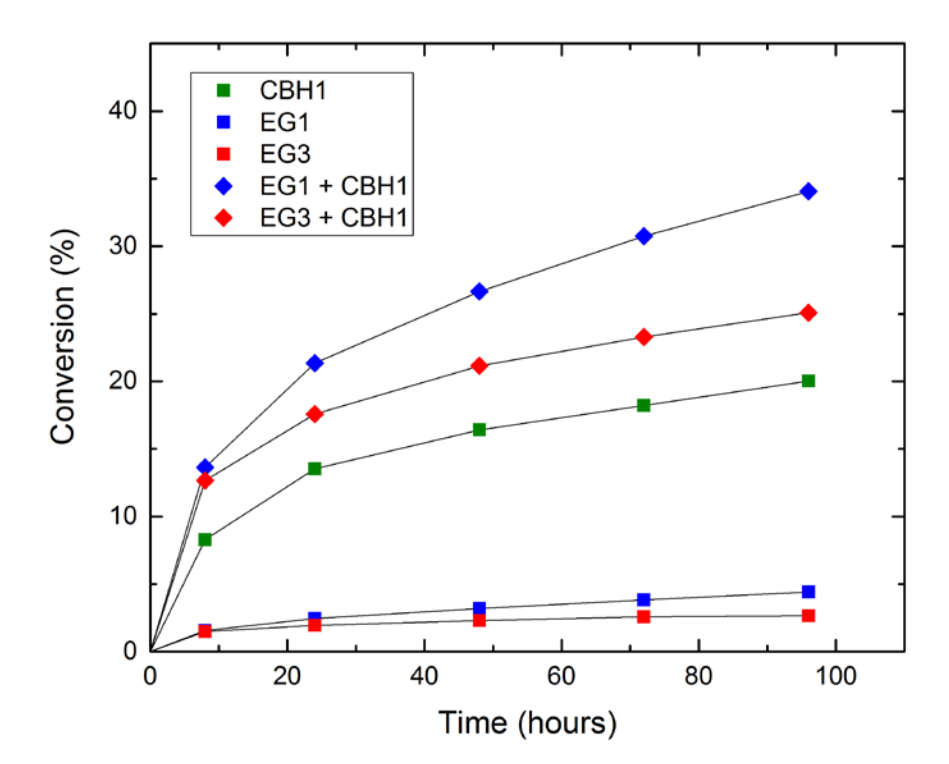


Figure 1 Activity measurements of monocomponent (squares) and 50/50 mixtures (diamonds) of CBH1 (green) with either EG1 (blue) or EG3 (red). Lines are shown to guide the eye.

#### Results

12 separate Avicel samples were digested by either mono- or bicomponent enzyme solutions (see Table 1), and aliquots were taken out at 5 time points for biochemical

analysis and 3 time points for imaging as described above. All samples had identical substrate and total enzyme loads at the beginning of the reaction. Conversion of substrate was calculated from the production of glucose and the progression over 96 hours is shown for selected samples in Figure 1. Five images were taken in the DICM for each sample at each time point. In the TEM 80-90 images were taken due to the much lower number of particles included in the image frame of this microscope at the magnification range used here. This resulted in 180 DICM and 2950 TEM micrographs (containing a total of approximately  $10^5$  and  $2\cdot10^5$  detectable particles, respectively), which were subjected to the semi-automated image analysis described above.

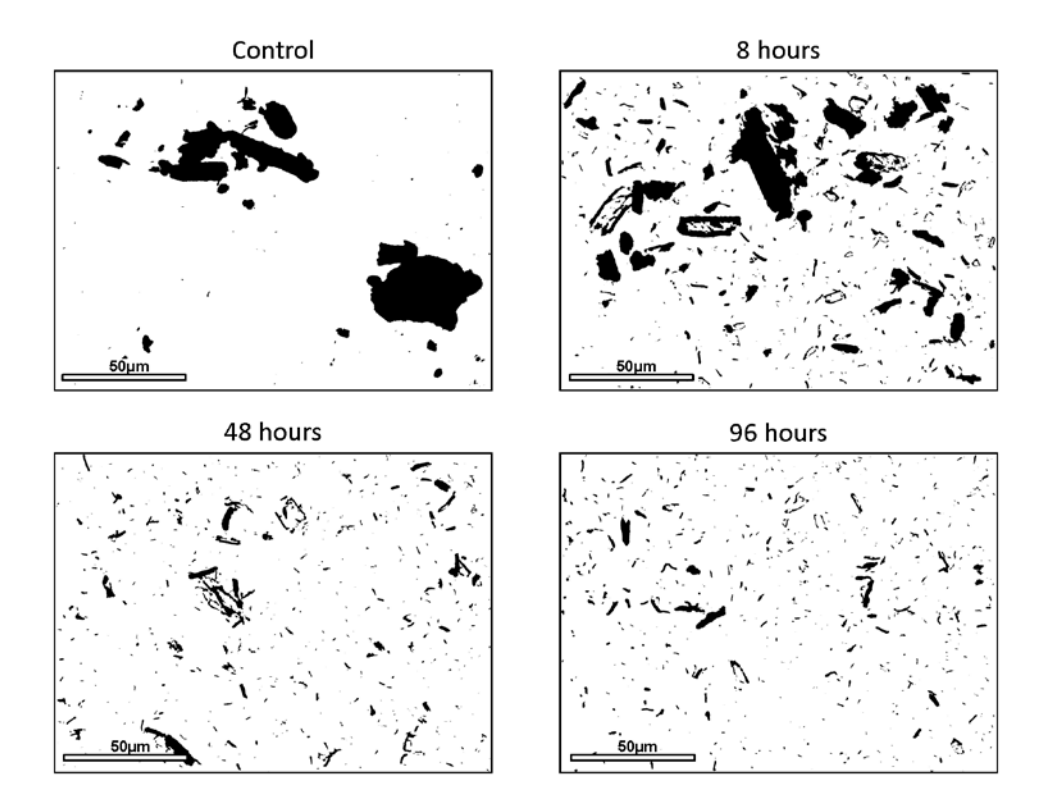


Figure 2 Detected particles in DICM micrographs of CBH1 digested Avicel after 8, 48 and 96 hours of hydrolysis, plus control incubated without enzyme for 8 hours (more details including raw images in Materials and methods and in the supplementary information). Scale bars =  $50\mu m$ .

#### Differential interference contrast microscopy

247

248

249

250

251

252

253

254

255

256

257

258

259

260

261

262

263

264

265

266

267

268

269

270

271

272

The differential interference contrast microscopy (DICM) images covered a field of view of 195 x146 µm with a pixel size of 122nm, and a typical micrograph contain hundreds of particles ranging from a single pixel to ~50um in length. Representative micrographs of CBH1 digested samples after 8, 48 and 96 hours of hydrolysis as well as an 8-hour control without added enzyme are shown in Figure 2. From visual inspection it is clear that the size distribution and number of particles change over time for this particular sample and similar trends were observed for all other samples (not shown). Generally we observed no obvious differences in the structural effects on this length scale among different enzymes and mixtures. while different samples could often be distinguished from each other at a given time point, all samples followed similar trends when various structural parameters were considered in relation to the degree of conversion. This does not imply that the effect of the different enzymes is identical, but rather that the variation in particle sizes and shapes was large enough that any difference between samples was impossible to distinguish by eye. However we did find that control samples without added enzyme contained considerably fewer particles than enzyme treated samples and that the number of observed particles increased with conversion at least until 10% conversion after which no correlation was found (Figure 5, top). There was also a slight decrease in mean particle size that is apparent in the representative micrographs shown in Figure 2. However, the measured lengths fell into a log-normal distribution, and as such the mean does not adequately describe the typical particle (supplementary material). When looking at the representative micrographs shown in Figure 2 it is clear that a relatively small number of large particles is present before the onset of the reaction, and that these break apart once enzyme is added. This was reflected in a slight decrease in the mean particle size (data not shown). However, as mentioned above the particle sizes were log-normal distributed and as such the mean

provides a very poor summary of the typical particle in a given sample. If medians were
considered instead of means neither the particle perimeter (not shown) nor the length
(Figure 3, top) changed with conversion. This might seem counter intuitive and at odds
with what is readily observable from micrographs in Figure 2. However, the fact that the
median particle length did not correlate with the degree of conversion was caused by
the vast majority of particles being relatively small and similar in shape and size. In
other words even though some very large particles obviously did break apart to form
much smaller fragments, these were so few in numbers that they hardly affected the
overall picture of the reaction mixture. Thus, if the 99th percentile lengths were plotted
against conversion we observed a highly significant, negative correlation (Table 2).
Conversely, for the 75th percentile, there was a very weak ( $R = -0.17$ ) but non-
significant correlation (Table 2), indicating that most of the size distribution did in fact
not change during conversion, even though the very largest particles did. To ensure that
this finding was not an artifact of the image analysis, we analyzed all samples with
sufficient residual volume after microscopy on a coulter counter. While the results in
terms of absolute values could not be compared between the two analyses, the
observations that median particle size was unchanged throughout the experiment and
that particle number increased initially but was unchanged during extended hydrolysis
were confirmed (see supplementary material).
To determine whether the shape of the particles changed we computed their circularity.
This size independent parameter, calculated as $4\pi \cdot area/perimeter^2$ , is a number
between 0–1 with 1 being a perfect circle. As seen in Figure 3 and Table 2 a somewhat
similar albeit not identical picture was seen for this measure: We found a moderate,
negative correlation for the median circularity, no significant correlation for the 25th
percentile and a moderate, positive correlation for the 1st percentile. Since we see a
strong, negative correlation between size and circularity (not shown) the results for the

1st percentile might reflect that the larger particles would often overlap, forming very non-circular aggregates as seen in the second and third panel of Figure 2. Conversely the shape of the typical particle, represented by the median circularity, became slightly less circular during conversion, which might be an indication of particle narrowing as previously reported for other cellulosic substrates (Boisset et al. 2000; Imai et al. 1998; Jeoh et al. 2013). For both length and circularity, the control samples were considerably different from enzyme treated samples irrespective of treatment time. Thus they were omitted from the correlation analysis and considered separately.

In summary the typical particle would not significantly shorten and only slightly narrow or in any other way change its general proportions on the µm length scale within the conversion range studied here —an observation which will be addressed in more detail below. Interestingly, this observation applied to all investigated enzymes and mixtures, which was in contrast to previous reports (reviewed in the introduction).

Table 2 Pearson correlation parameters for selected percentiles of particle length and circularity.

Note that the control samples without added enzyme were excluded from the regression analysis.

	Median		25th/75th percentile*		1st/99th percentile**	
	Correlation	Significance	Correlation	Significance	Correlation	Significance
Length	Very weak (R = 0.073)	None (p = 0.199)	Very weak (R = -0.17)	None (p = 0.344)	Moderate (R = -0.58)	Very high (p < 0.001)
Circularity	Moderate (R = -0.49)	High (p = 0.004)	Weak (R = -0.24)	None (p = 0.186)	Moderate (R = 0.46)	High (p = 0.007)

<sup>\* 25</sup>th percentile for circularity, 75th for length. \*\* 1st percentile for circularity, 25th for length

One might expect that the typical particle size would decrease as more and more of the cellulose was solubilized, especially as this coincided with an increase in the number of particles. However, from a qualitative, visual survey of the micrographs it is apparent that a small number of relatively large particles (approximately 50µm) were present at low degrees of conversion but disappeared as the reaction progressed (Figure 2). This

320

321

322

323

324

325

326

327

328

Figure 3 Particle length (left) and circularity (right) determined as the Feret's diameter measured with FIJI in DICM images plotted against conversion at 3 time points for 12 different digestions (control (black circles), CBH1 (green), EG1 (blue) and EG3 (red) alone (squares) or in 4 different mixing ratios (all represented by diamonds), see Table 1). Linear regression with 95% confidence bands is shown in dark grey. Top panels show median values, middle panels show 75th percentile length and 25th percentile circularity, bottom panels show 99th percentile length and 1st percentile circularity. Note that the control samples without added enzyme were excluded from the regression analysis. See text for further details.

#### Transmission electron microscopy

330

331

332

333

334

335

336

337

338

339

340

341

342

343

344

345

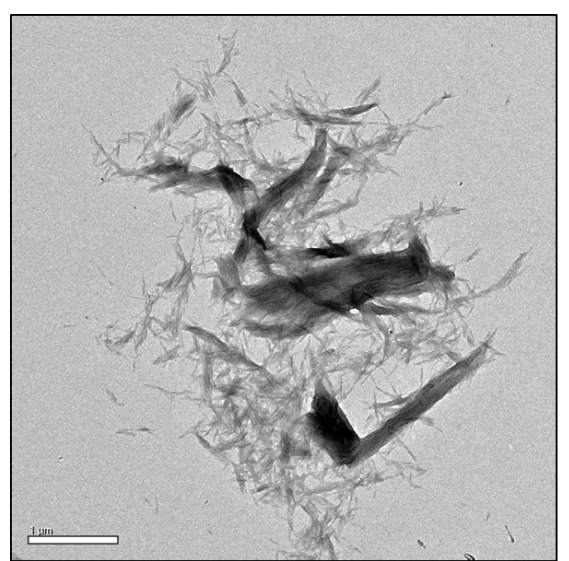
346

347

348

349

According to the DICM analysis the vast majority (>90%) of the observed particles had a length of less than 5  $\mu$ m. When studying the samples in the TEM we observed that the particles from 1-5 um exhibited very diverse morphologies. Many particles were surrounded by tiny fibrils or subparticles, some less than 10 nm wide but with a length of up to one µm and many of them overlapping to form relatively large aggregates (Figure 4). Some particles appeared diffuse and still others appeared condensed with a clearly defined perimeter. Importantly, no clear qualitative distinction between samples was possible because of this heterogeneity; all the investigated samples (including control samples without enzyme added) contained some examples of all particle morphologies and no systematic changes with time or enzyme mixture could be identified by visual inspection. This is not to say that the different samples looked similar per se or that individual particles did not change during the hydrolysis. Rather, the morphologies present in each individual sample were so diverse, that the overlap between samples made unaided distinction impossible. As seen in Figure 4 the individual subparticles could not be singled out in the automated analysis and for this reason we were unable to quantify structural parameters on a particle level as we did with DIC micrographs. Rather, for the TEM micrographs, we determined the total perimeter and area of every identified particle in a single micrograph. This resulted in 80-90 replicates (corresponding to the number of images) for each sample.



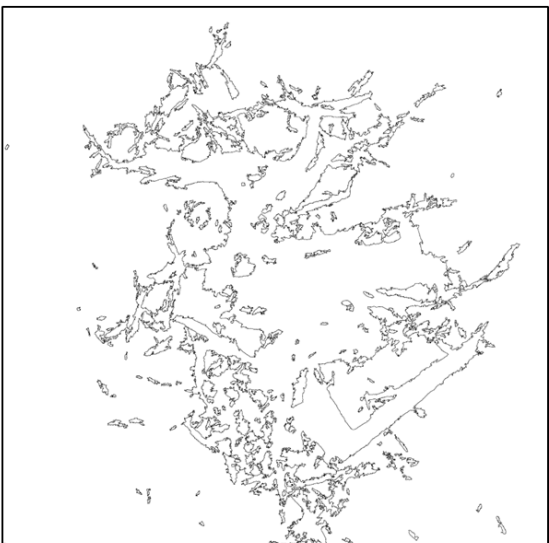


Figure 4 TEM micrograph of CBH1 digested Avicel after 8 hours of hydrolysis before image processing (left) and outlines of identified particles (right). Most sub-fibrils overlap making distinction between them impossible. Scale bar =  $1\mu m$ .

#### Particle surface area and roughness

Micrographs present a 2D projection of particles settled on a slide or a sample grid, and based on this we cannot directly determine 3D structural information. However the hydrolysis took place in bulk suspension before the particles settled on the imaging support. Unless there was a connection between enzyme target sites and how the cellulose particles settled on the support, the particles will be randomly oriented and the sizes and shapes of their 2D projection will presumably suffice as an approximation of the 3D surface parameters. We argue that this is the case in the present study even though a thorough exploration is beyond the current scope. Using the measured length and width of the particles observed in DICM and assuming a prolate spheroid shape we approximated apparent surface areas as follows

$$A = 2\pi a^2 + \frac{2\pi ac}{e} \cdot \sin^{-1}(e)$$

where c is half the measured length, a is half the measured width and e is  $\sqrt{c^2-a^2}\cdot c^{-1}$  (for more details see supplementary material)(Zwillinger 1996). The apparent surface area for each sample was calculated and as seen from Figure 5, this value increased during the first  $\sim 10\%$  conversion and then gradually decreased throughout the investigated conversion range. In contrast to the median values reported above – which gives information about the size and shape of the typical particle in a sample – the total surface area per micrograph is a relative measure of the "concentration" of substrate. With that in mind our results indicated that even though the  $\mu$ m scale size and shape of a typical Avicel particle was similar throughout the reaction, the apparent total surface area in the sample did change with conversion.

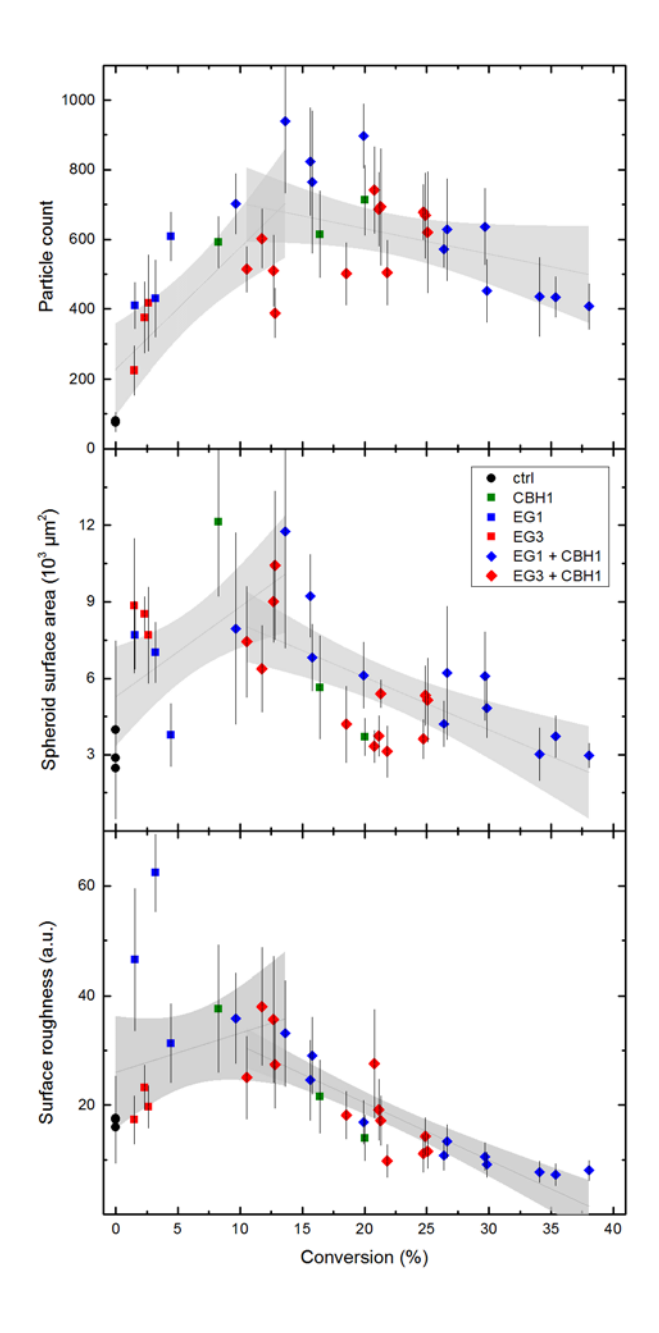


Figure 5 Average number of particles per DICM micrograph (top), average surface area calculated from DICM measurements (middle) and median surface roughness determined by TEM (bottom) all plotted against degree of conversion. Error bars represent standard deviation for 5 analytical replicates in the two uppermost panels and median absolute deviation in the bottom panel ( $n \approx 80$ -90). All three measures increase during the first 10-15% conversion, at which point the number of detected particles stay roughly constant while the surface area and – roughness start to decrease (linear regression with 95% confidence bands shown in gray. See Table 3 for non-linear correlation parameters). Symbols and colors have the same meaning as in Figure 3.

As described above, TEM revealed a high prevalence of composite structures comprising many small overlapping subparticles. We could not distinguish the individual subparticles in the automated analysis therefore we used the total perimeter and area in each micrograph to evaluate the relative surface roughness. We calculated the perimeter of a hypothetical circle with the same area as the total measured area for each micrograph (supplementary material). We then used the ratio of the observed perimeter to this theoretical perimeter as a relative measure of surface roughness on the nm scale. When plotted against overall substrate conversion (Figure 5) we observed a similar pattern to the approximated surface area calculated from DICM data; a slight initial increase followed by a marked decrease until it apparently leveled off at the highest conversions studied here (~30%). The progressions in particle count, surface area and surface roughness depicted in Figure 5 were all non-monotone, and neither of them was suited for any parameterized regression methods. Using a Hoeffding's independence test we were able to verify that the variations in the determined values were significantly dependent on the degree of conversion (p < 0.001 in all three cases). To analyze the correlation in detail we identified a maximum in all three data sets around 10-15% conversion and carried out separate correlation analyses for the data before and after this maximum. The results confirm our intuitive interpretation of the data, i.e. all three measures increased until 10-15% conversion, at which point the particle count stayed roughly constant while the surface area and - roughness started to decrease (see Figure 5 and Table 3).

385

386

387

388

389

390

391

392

393

394

395

396

397

398

399

400

401

402

403

404

405

406

Table 3 Spearman's correlation parameters for plots in Figure 5. Since the progressions in all three values were non-monotone the data set was divided into two parts which were analyzed separately.

	Conversion	on 0 - 15%	Conversion 10 - 40%		
	Correlation	Significance	Correlation	Significance	
Particle count	Strong (ρ = 0.78)	Very high (p < 0.001)	Weak (ρ = -0.30)	None (p = 0.14)	

Surface area	Moderate $(\rho = 0.59)$	Moderate (p = 0.0155)	Strong (ρ = -0.68)	Very high (p < 0.001)	
Roughness	Moderate (ρ = 0.56)	Moderate (p = 0.029)	Very strong $(\rho = -0.91)$	Very high (p < 0.001)	

409

410

411

412

413

414

415

416

417

418

419

420

421

422

423

424

425

426

Based on the results of the automated analysis we suggest that sub-µm fibrils are predominantly present in the early stages of the reaction. This would indicate that the actual surface area as experienced by an enzyme is decreasing in a manner, which is not readily observed on the length scale used in the DICM analysis. The relative surface roughness determined by TEM is a dimensionless number, equivalent to actual surface area (nm resolution) per approximated surface area (µm resolution). Thus we used the relative surface roughness determined by TEM to correct the surface area calculated from DICM measurements by multiplying these two values. The resulting parameter was used to estimate the total surface area within the studied samples. Plotting the rate of the reaction for CBH1 alone and in mixtures against this measure gave a strong linear correlation as seen in Figure 6 (R = 0.81, p < 0.0001). Because the volume of sample in the microscope image frame is unknown we were unable to relate the determined surface area to the amount of cellulose, which makes validation by independent measurement or literature reference impossible. However we can roughly estimate the liquid volume in a single DIC micrograph to be on the order of  $10^{-4} \, \mu l$  which, at a cellulose concentration of 10 µg/µl and specific surface area of 1-25 m<sup>2</sup>/g Avicel (Marshall and Sixsmith 1975), puts the expected area at 1-25 mm<sup>2</sup> per image. Considering the approximations and measuring uncertainties we deem this to be in relatively good agreement with our results (see Figure 6).

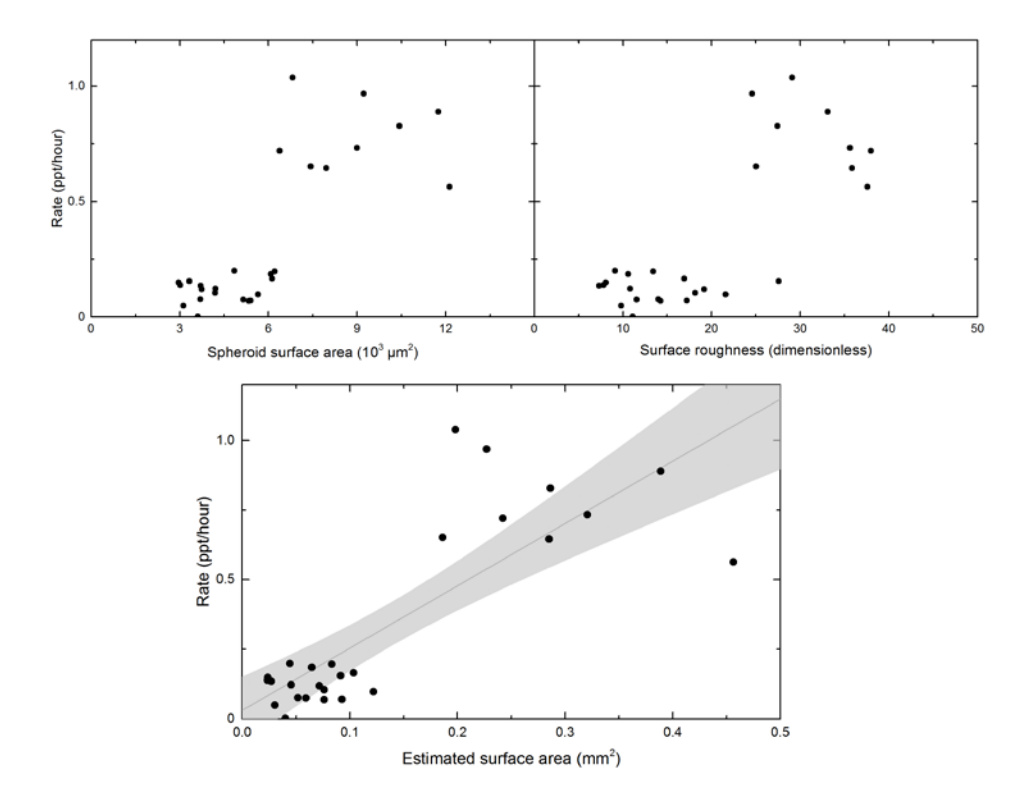


Figure 6 Reaction rate (percentage points per hour) plotted against calculated surface area determined by DICM (top, left) and surface roughness determined by TEM (top, right) as described in the text. The reaction rate in samples digested by CBH1 alone or in mixtures correlated linearly (dotted line) to the accessible surface area in the microscope field of view under the conditions

studied here (bottom panel, 95% confidence bands shown in gray).

#### **Discussion and Conclusions**

We have used a combination of DICM and TEM to observe and measure changes in Avicel particle size and shape during enzymatic hydrolysis. We developed a method to perform a reliable and unbiased quantitation of size, shape and surface roughness of these particles on a  $\mu$ m-nm scale. Based on analyses of 180 DICM and 2950 TEM micrographs comprising a total of more than 300,000 particles we found that for the enzymes studied here, the changes in shape and surface structure of Avicel was not determined by the type of enzyme or composition of enzyme mixtures but rather they depended on the degree of conversion that had taken place at the time of observation.

We observed a marked increase in particle count with initial conversion but no change
in the median size of Avicel particles on a $\mu m$ scale. This somewhat counter intuitive
result (which was independently confirmed by coulter counter analysis – see
supplementary material) indicates that even though the very largest particles were
dramatically altered by enzymatic degradation, the general size distribution was by and
large unaltered during the experiment. Furthermore we observed only a slight change in
the shape of particles on this scale. On a nm scale we observed a very large degree of
heterogeneity in the surface structure of Avicel, but by increasing the sampling size we
obtained reliable data on the surface roughness at this scale. Note that the data
acquisition was done blind to avoid any bias in the selection of captured particles. When
quantifying changes in relative surface area on both $\mu\text{m}$ and nm scale we found a slight
initial increase followed by a continuous decrease throughout the studied range of
conversion. Based on these observations we suggest that most particles were in the
form of large superparticle aggregates prior to enzyme addition and that the initial
activity of the studied enzymes rapidly broke these aggregates apart to form a large
number of much smaller particles. In the following (still early) phase of reaction a large
fraction of the cellulose was in the form of sub- $\!\mu m$ fibrils that were difficult to
distinguish by DICM. These fibrils appear to be relatively easy to degrade and their
presence decreased as the hydrolysis progressed, leaving compact (possibly
recalcitrant) particles behind in accordance with previous observations (Chanzy et al.
1983; Imai et al. 1998; Jeoh et al. 2013). By combining the DICM and TEM
measurements we obtained a relative measure of the available surface area over the
course of hydrolysis and, as was the case for the two values separately, this number
initially increased slightly but subsequently decreased as the hydrolysis progressed to
around 30% conversion where it leveled off (not shown). It should be noted that for
experimental reasons our analysis does not go beyond this conversion and that the
results might not hold for higher degrees of conversion. Nonetheless, our observation is

469	in agreement with the degree of conversion at which Bansal and colleagues determined
470	a leveling off of both accessibility and hydrolysability (Bansal et al. 2012). Furthermore
471	we found that the rate of reaction for CBH1 alone and in mixtures was closely correlated
472	to the relative accessible surface area in the conversion range studied here (Figure 6).
473	Based on these findings we conclude that surface alterations on both $\mu m$ and $nm$ length
474	scales do indeed impact the rate loss that is unambiguously observed for cellulases in
475	their hydrolysis of cellulose.
476	Electronic supporting material available
477	Supporting information includes details and examples on the automated image
478	processing and analysis procedures for both DICM and TEM micrographs. Furthermore
479	it includes results from coulter counter measurements of particle size distribution and
480	number of particles in the reaction mixture. Finally, also found in the supporting
481	information is details on the distribution of DICM data and on the geometry behind the
482	conversion from 2D to 3D structural information.
483	References
484 485 486	Antal MJ, Jr. (1985) Biomass pyrolysis: A review of the literature part 1 - carbohydrate pyrolysis. In: Böer KW, Duffie JA (eds) Advances in solar energy. Springer New York, pp 61-111. doi:10.1007/978-1-4684-8992-7_3
487 488 489	Arantes V, Saddler JN (2011) Cellulose accessibility limits the effectiveness of minimum cellulase loading on the efficient hydrolysis of pretreated lignocellulosic substrates. Biotechnology for Biofuels 4(3)
490 491	Bansal P, Hall M, Realff MJ, Lee JH, Bommarius AS (2009) Modeling cellulase kinetics on lignocellulosic substrates. Biotechnology Advances 27(6): 833-848
492 493 494	Bansal P, Vowell BJ, Hall M, Realff MJ, Lee JH, Bommarius AS (2012) Elucidation of cellulose accessibility, hydrolysability and reactivity as the major limitations in the enzymatic hydrolysis of cellulose. Bioresour Technol 107: 243-250
495 496 497	Boisset C, Fraschini C, Schülein M, Henrissat B, Chanzy H (2000) Imaging the enzymatic digestion of bacterial cellulose ribbons reveals the endo character of the cellobiohydrolase cel6a from humicola insolens and its mode of synergy with

498 499	cellobiohydrolase cel7a. Applied and environmental microbiology 66(4): 1444- 1452
500 501 502	Bubner P, Dohr J, Plank H, Mayrhofer C, Nidetzky B (2012) Cellulases dig deep - in situ observation of the mesoscopic structural dynamics of enzymatic cellulose degradation. Journal of Biological Chemistry 287(4): 2759-2765
503 504	Bubner P, Plank H, Nidetzky B (2013) Visualizing cellulase activity. Biotechnology and bioengineering 110(6): 1529-1549
505 506	Chanzy H, Henrissat B (1985) Undirectional degradation of valonia cellulose microcrystals subjected to cellulase action. FEBS Letters 184(2): 285-288
507 508 509	Chanzy H, Henrissat B, Vuong R, Schülein M (1983) The action of 1,4-β-d-glucan cellobiohydrolase on valonia cellulose microcrystals. FEBS Letters 153(1): 113-118
510 511 512 513	Ciesielski PN, Wang W, Chen X, Vinzant TB, Tucker MP, Decker SR, Himmel ME, Johnson DK, Donohoe BS (2014) Effect of mechanical disruption on the effectiveness of three reactors used for dilute acid pretreatment of corn stover part 2:  Morphological and structural substrate analysis. Biotechnol Biofuels 7: 47
514 515 516	Donohoe BS, Resch MG (2015) Mechanisms employed by cellulase systems to gain access through the complex architecture of lignocellulosic substrates. Curr Opin Chem Biol 29: 100-107
517 518 519 520	Eriksson T, Karlsson J, Tjerneld F (2002) A model explaining declining rate in hydrolysi of lignocellulose substrates with cellobiohydrolase i (cel7a) and endoglucanase (cel7b) of trichoderma reesei. Applied Biochemistry and Biotechnology 101: 41 60
521 522	Grethlein HE (1985) The effect of pore-size distribution on the rate of enzymatic-hydrolysis of cellulosic substrates. Bio-Technol 3(2): 155-160
523 524	Hall M, Bansal P, Lee JH, Realff MJ, Bommarius AS (2010) Cellulose crystallinity - a key predictor of the enzymatic hydrolysis rate. FEBS Journal 277(6): 12-12
525 526 527 528	Hong J, Ye X, Zhang YHP (2007) Quantitative determination of cellulose accessibility to cellulase based on adsorption of a nonhydrolytic fusion protein containing cbm and gfp with its applications. Langmuir: the ACS journal of surfaces and colloids 23(25): 12535-12540
529 530 531	Imai T, Boisset C, Samejima M, Igarashi K, Sugiyama J (1998) Unidirectional processive action of cellobiohydrolase cel7a on valonia cellulose microcrystals. FEBS Letters 432(3): 113-116
532 533 534	Jalak J, Väljamäe P (2010) Mechanism of initial rapid rate retardation in cellobiohydrolase catalyzed cellulose hydrolysis. Biotechnology and Bioengineering 106(6): 871-883
535 536 537	Jeoh T, Ishizawa CI, Davis MF, Himmel ME, Adney WS, Johnson DK (2007) Cellulase digestibility of pretreated biomass is limited by cellulose accessibility. Biotechnology and bioengineering 98(1): 112-122

538 539	Jeoh T, Santa-Maria MC, O'Dell PJ (2013) Assessing cellulose microfibrillar structure changes due to cellulase action. Carbohydrate Polymers 97(2): 581-586
540 541 542	Kapur JN, Sahoo PK, Wong AKC (1985) A new method for gray-level picture thresholding using the entropy of the histogram. Computer Vision, Graphics, and Image Processing 29(3): 273-285
543 544	Levine SE, Fox JM, Blanch HW, Clark DS (2010) A mechanistic model of the enzymatic hydrolysis of cellulose. Biotechnology and Bioengineering 107(1): 37-51
545 546 547 548	Luterbacher JS, Moran-Mirabal JM, Burkholder EW, Walker LP (2015) Modeling enzymatic hydrolysis of lignocellulosic substrates using confocal fluorescence microscopy i: Filter paper cellulose. Biotechnology and Bioengineering 112(1): 21-31
549 550	Marshall K, Sixsmith D (1975) Some physical characteristics of microcrystalline cellulose .1. Powders for pharmaceutical use. Drug Dev Commun 1(1): 51-71
551 552	Payne CM, Knott BC, Mayes HB, Hansson H, Himmel ME, Sandgren M, Stahlberg J, Beckham GT (2015) Fungal cellulases. Chem Rev 115(3): 1308-1448
553 554 555	Praestgaard E, Elmerdahl J, Murphy L, Nymand S, McFarland KC, Borch K, Westh P (2011) A kinetic model for the burst phase of processive cellulases. FEBS Journal 278(9): 1547-1560
556 557 558	Resch MG et al. (2014) Clean fractionation pretreatment reduces enzyme loadings for biomass saccharification and reveals the mechanism of free and cellulosomal enzyme synergy. ACS Sustainable Chemistry & Engineering 2(6): 1377-1387
559 560 561	Rogers EW, Zack GW, Latt SA (1977) Automatic measurement of sister chromatid exchange frequency. The Journal of Histochemistry and Cytochemistry 25(7): 741-753
562 563	Schindelin J et al. (2012) Fiji: An open-source platform for biological-image analysis. Nat Methods 9(7): 676-682
564 565 566	Sprey B, Bochem H-P (1992) Effect of endoglucanase and cellobiohydrolase from trichoderma reesei on cellulose microfibril structure. FEMS Microbiology Letters 97(1-2): 113-117
567 568 569 570	Wang J, Quirk A, Lipkowski J, Dutcher JR, Clarke AJ (2013) Direct in situ observation of synergism between cellulolytic enzymes during the biodegradation of crystalline cellulose fibers. Langmuir: the ACS journal of surfaces and colloids 29(48): 14997-15005
571 572	Westh P, Kari J, Olsen JP, Borch K, Jensen K, Krogh KBRM (2014) Cellobiohydrolase variants and polynucleotides encoding same. Patent no. WO 2014064115 A1
573 574	Yang B, Willies DM, Wyman CE (2006) Changes in the enzymatic hydrolysis rate of avicel cellulose with conversion. Biotechnology and Bioengineering 94(6): 1122-1128
575 576 577	Zhang YHP, Lynd LR (2004) Toward an aggregated understanding of enzymatic hydrolysis of cellulose: Noncomplexed cellulase systems. Biotechnology and Bioengineering 88(7): 797-824

Zwillinger D (ed) (1996) Crc standard mathematical tables and formulae. 30th edn. CRC Press, Boca Raton, Florida

# Supplementary material

## 2 Image processing – DICM:

Figure S1 shows a step-by-step review of the automated processing of a representative DICM micrograph as carried out in Fiji. The sample was Avicel digested with Cel7A for 8 hours. Contrast was increased by the "Enhance Contrast" function with saturated pixels set to 0.5% and "Normalize" option checked (A). Next the image was converted to binary by (B) applying the "Yen" threshold algorithm (Kapur et al. 1985), and the outermost 60 pixels along all four edges were cropped away (C). Finally the "Fill Holes" command was applied (D) and the particle perimeters and areas were determined by the "Analyze Particles" function (E).

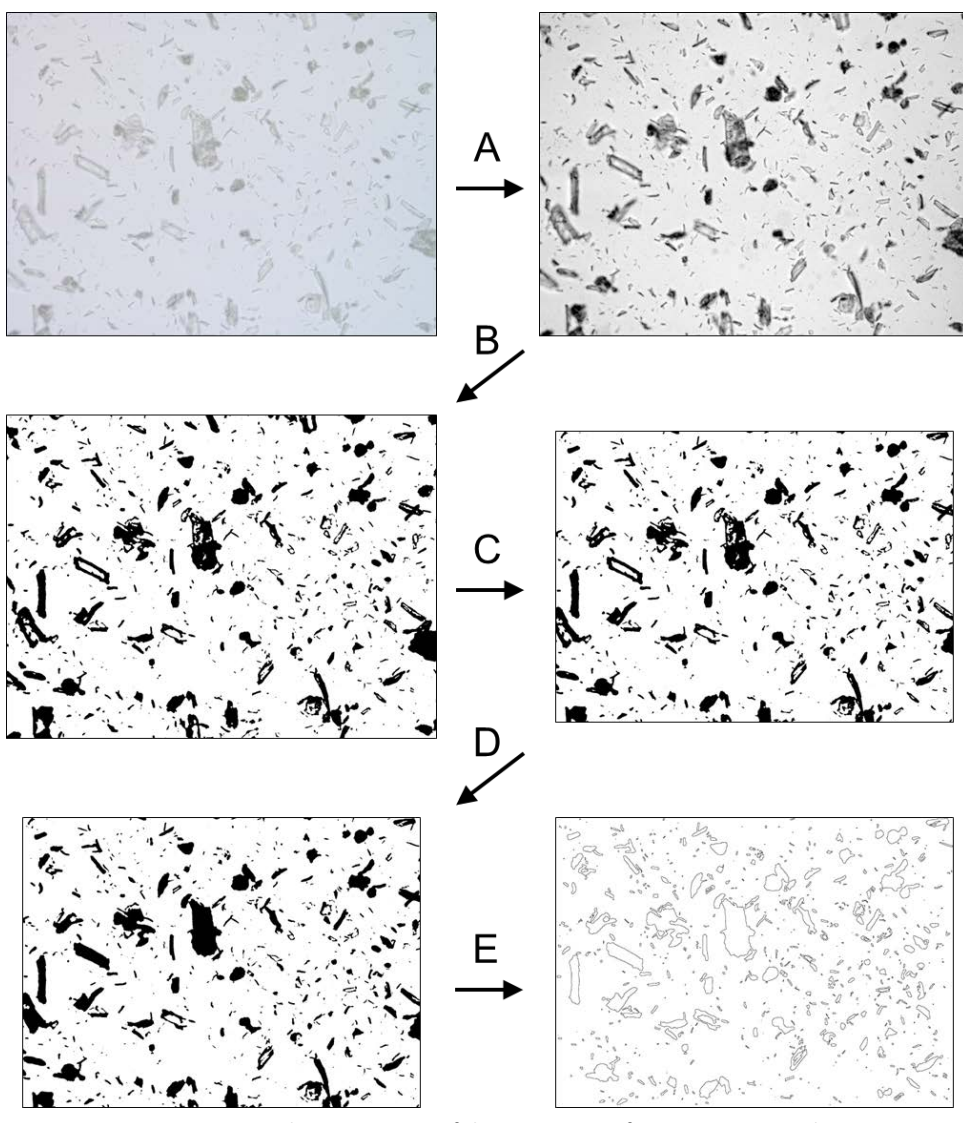


Figure S1 Step-by-step review of the processing of a DICM micrograph.

9 10

3

4

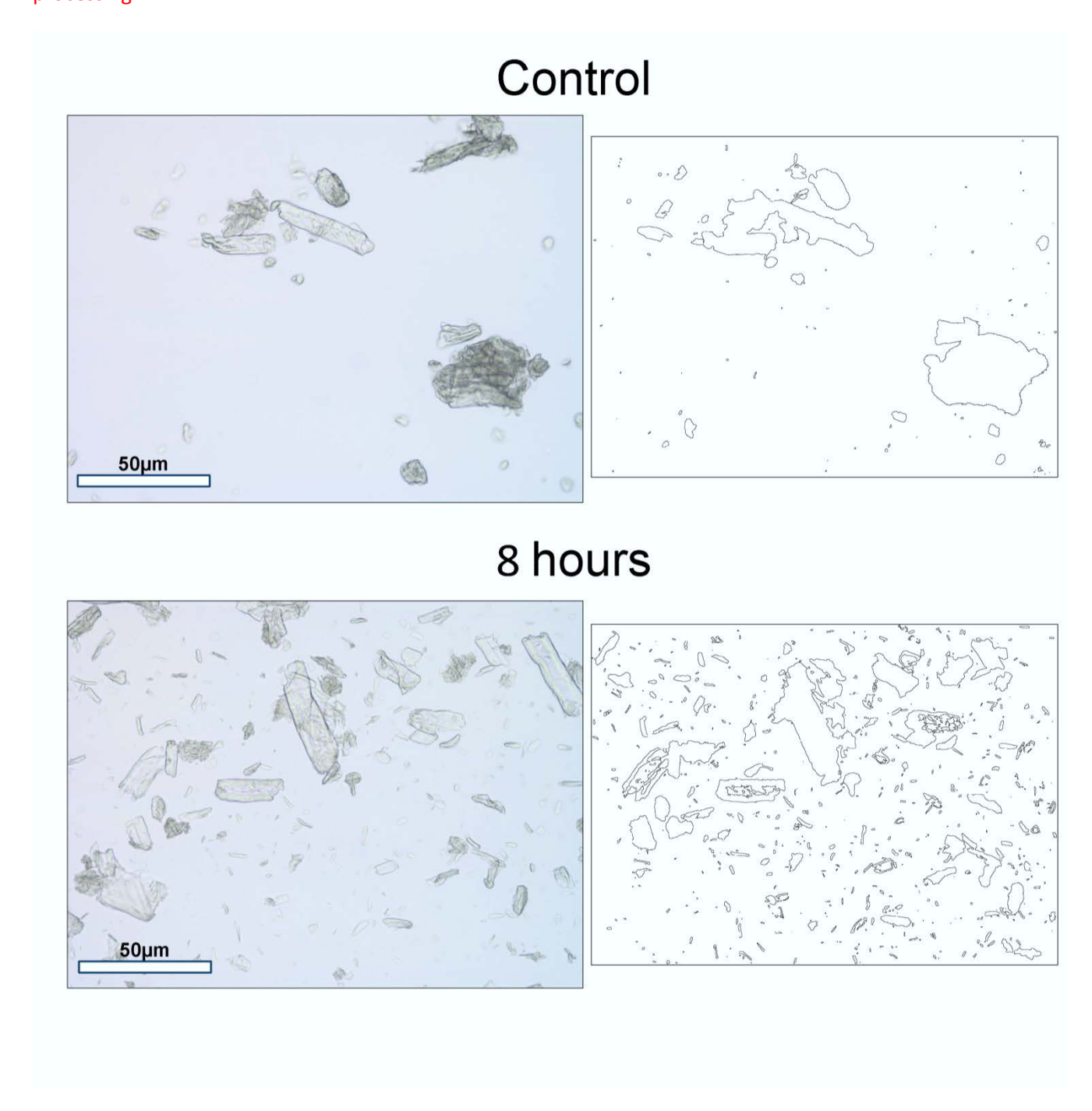
5

6

7

# 2 Representative DIC micrographs:

- 3 Figure S2 shows the same representative DIC micrographs as Figure 2 in the main text before and after image
- 4 processing



# 48 hours 50µm 96 hours 50µm

2 Figure S2 Representative micrographs shown in Figure 2 in the main text before and after processing.

1

## Coulter counter results

Figure S3 shows results from coulter counter analysis of particle sizes analogously to Figure 3 in the main text. The observation from DICM that the median size did not change with conversion is even more pronounced for this measurement. Thus no correlation between diameter and conversion was observed for even for the 99th percentile (not shown), but for the 99.99th percentile a moderate correlation appeared (Figure S3, bottom). Correlation parameters are shown in Table S1.

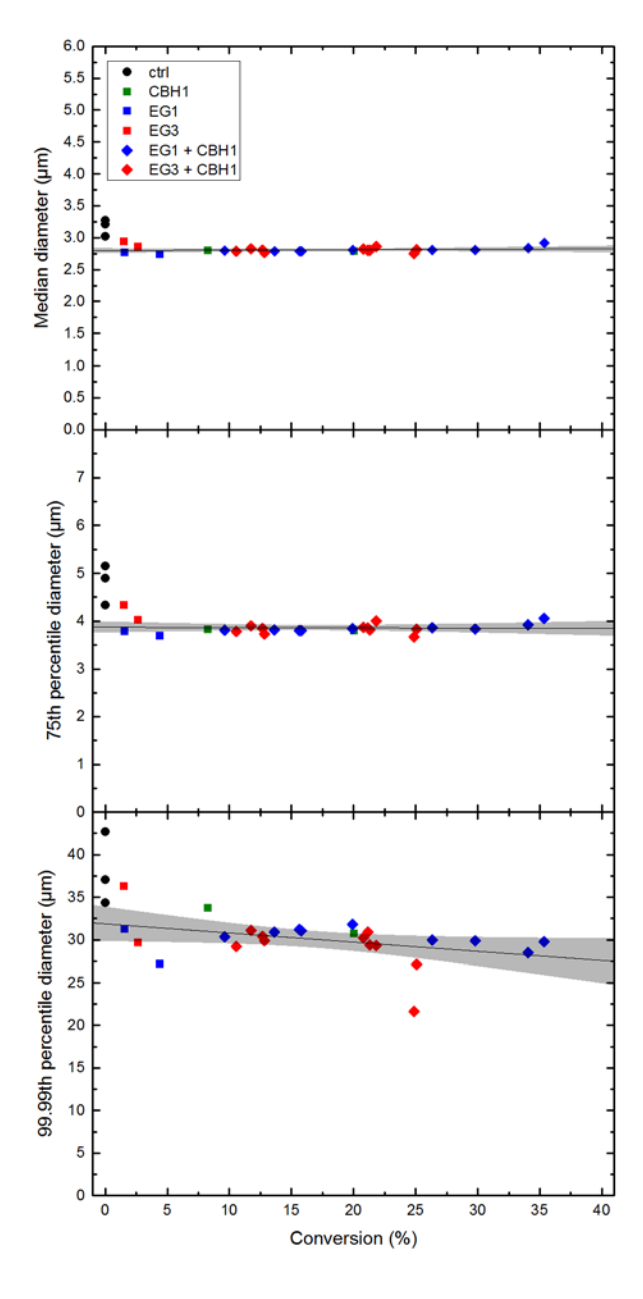


Figure S3 Median (top), 75th percentile (middle) and 99.99th percentile (bottom) particle diameter measured on coulter counter. Symbols and colors have the same meaning as in Figure 3 in the main text.

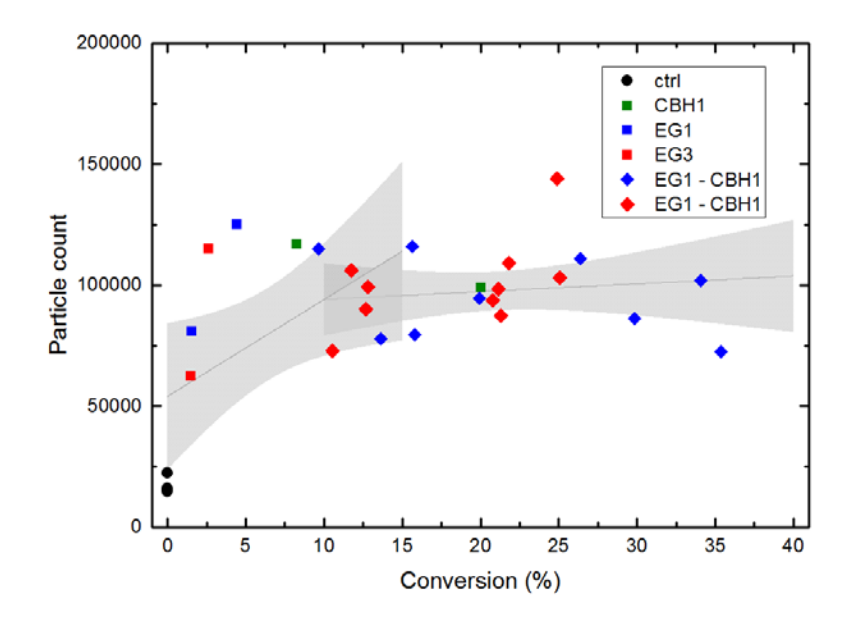
7

Table S1 Correlation analysis for particle diameter measured on coulter counter

	Median		75th percentile		99.99th percentile	
	Correlation	Significance	Correlation	Significance	Correlation	Significance
Length	Very weak (R = 0.14)	None (p = 0.51)	Very weak (R = -0.05)	None (p = 0.82)	Moderate (R = -0.40)	Moderate (p = 0.046)

4 5 6

Figure S4 shows the particle count determined by coulter counter plotted against conversion. Correlation parameters for the same data are shown in Table S2. In agreement with microscopy results reported in the main text, the number of particles increases during the early phase of the reaction but is unchanged throughout the rest of the experiment.



8 9

Figure S4 Particle count determined by coulter counter plotted against conversion. Symbols and colors have the same meaning as in Figure 3 in the main text.

11

12

10

Table S2 Correlation analysis for particle count determined by coulter counter

	Conversion 0 - 15%		Conversion 10 - 40%	
_	Correlation	Significance	Correlation	Significance
Particle count	Moderate $(\rho = 0.47)$	Low (p = 0.088)	Very weak (ρ = 0.14)	None (p = 0.57)

# Image processing – TEM:

 Figure S5 shows a step-by-step review of the processing of a representative image from TEM. The sample was digested with CBH1 for 8 hr. Noise was minimized by the "Remove Outliers" option (A), which changes the value of any pixel to the median of all pixel values in a surrounding block of designated size (here, 10x10 pixel) if that pixel deviates from that median by more than a specified value (1x standard deviation). Subsequently the images were converted from grayscale to a binary mask by applying the "Triangle" threshold method (Rogers et al. 1977) (B) and the perimeter and area of the individual particles were analyzed by Fiji's "Analyze Particles" procedure (C). The mask was also black/white inverted (D) allowing for a similar analysis of the holes (E). The resulting two data files were combined with a script in Matlab (R2013a v 8.1.0.604, Natick, Ma, USA), hence (F) is included for illustrative purposes.

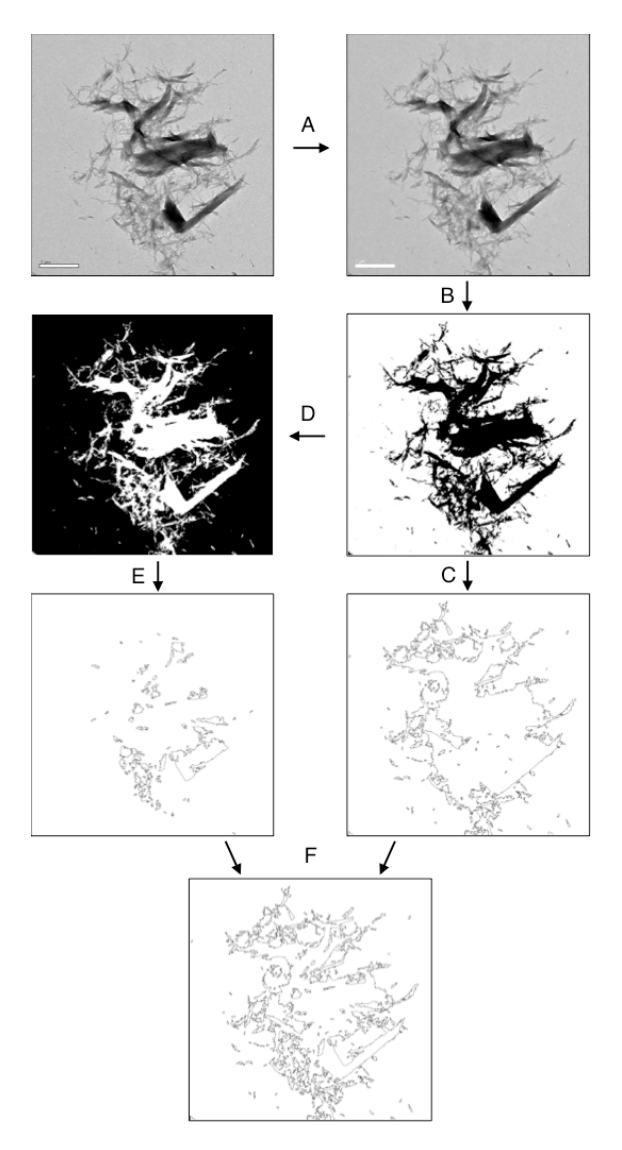


Figure S5 Step-by-step review of the processing of a TEM micrograph (See text for details).

# Distribution of particle sizes

The particle lengths, widths, areas and perimeters measured in DICM did not follow a normal distribution. Plots and analyses shown in Figure S6 are for particle length after 8 hours digestion with CBH1, but similar patterns applied for all data. Data was clearly skewed with most observations falling into a relatively small quantile combined with a long "tail" of observations over a very large size distribution (histogram in Figure S6, left). When data was plotted against a theoretical normal distribution in a normal probability (Q-Q) plot, deviation from linearity clearly confirmed, that the data was not normal distributed. When the same plots were made for the log-transformed data (Figure S6, right), both histogram and Q-Q plot confirmed that data fell into a log-normal distribution.

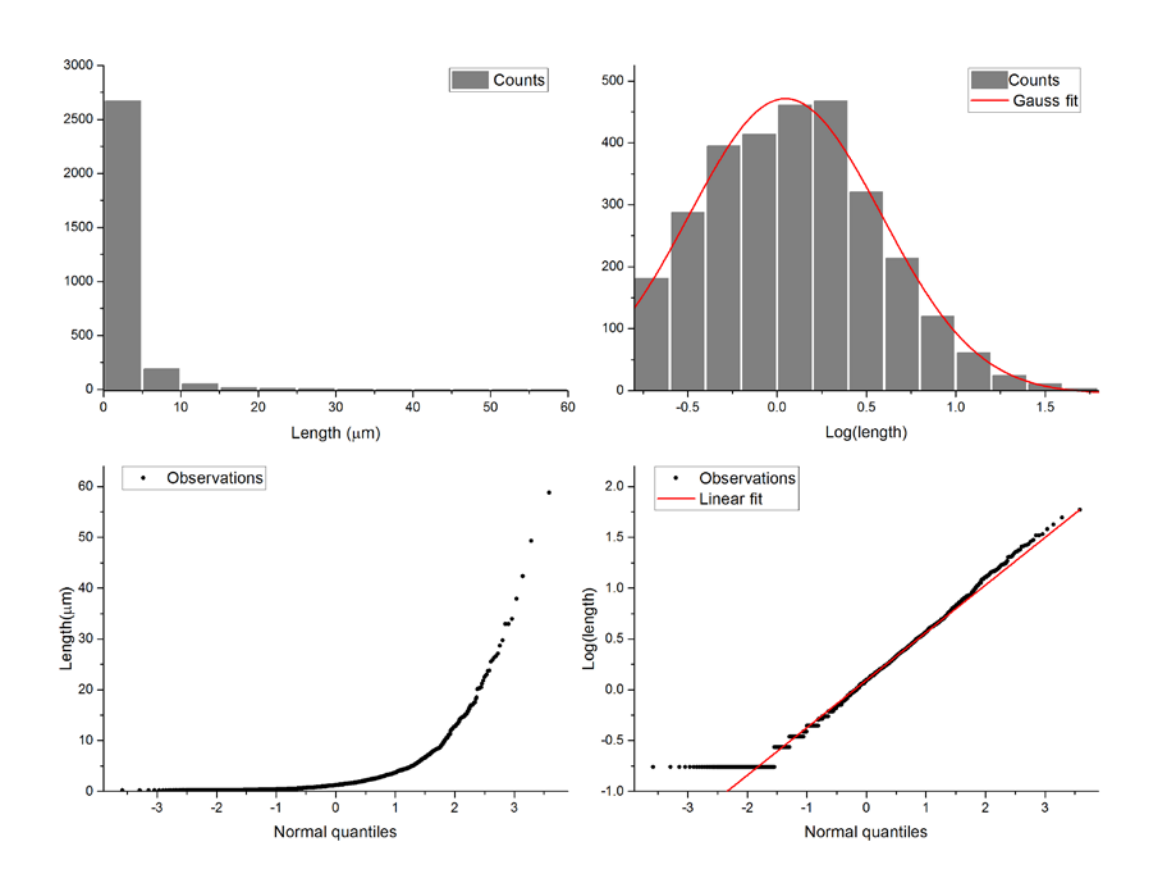


Figure S6 Left: Histogram and normal probability (Q-Q) plot of Avicel particle lengths after 8 hours of digestion by CBH1. From the histogram it is clear the data is skewed with most observations falling between 0 and 5  $\mu$ m but some being as high as 60  $\mu$ m. Right: Same as left after log-transformation of data. The histogram fits a normal distribution reasonably well and the log-normal distribution of the data was confirmed by the linear correlation with a theoretical normal distribution in the Q-Q plot. Results for the smallest particles were poorly resolved probably due to the image resolution.

#### 1 Estimating surface area from 2D projection of a particle

- 2 In the analysis presented in the main text we assume that the surface of avicel particles can be approximated
- 3 from DICM observations by treating each particle as a prolate spheroid, i.e. the 3-dimensional structure
- 4 obtained by rotating an ellipse about its longest axis (see Figure S7).
- 5 The surface area of a spheroid can be calculated as follows (Zwillinger 1996):

6 
$$A = 2\pi a^2 + \frac{2\pi ac^2}{\sqrt{c^2 - a^2}} \cdot \sin^{-1}\left(\frac{\sqrt{c^2 - a^2}}{c}\right) = 2\pi a^2 + \frac{2\pi ac}{e} \cdot \sin^{-1}\left(e\right)$$

7 Where  $e = \sqrt{c^2 - a^2} \cdot c^{-1}$  while a and c are the minor and major radii, respectively.

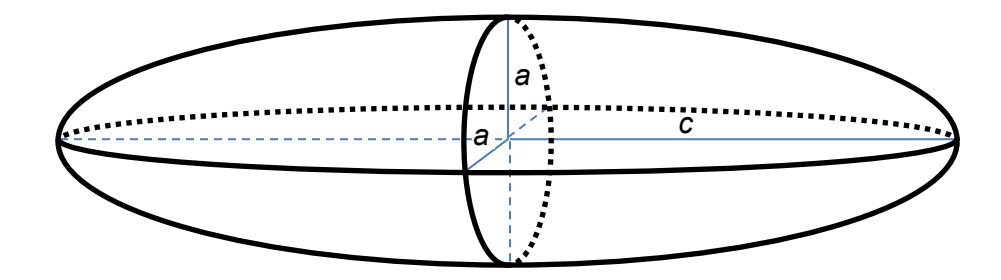


Figure S7 Particle shape was approximated as a prolate spheroid.

9

11 12

13

14

8

#### References

Kapur JN, Sahoo PK, Wong AKC (1985) A new method for gray-level picture thresholding using the entropy of the histogram. Computer Vision, Graphics, and Image Processing 29(3): 273-285

Zwillinger D (ed) (1996) Crc standard mathematical tables and formulae. 30th edn. CRC-Press, Boca Raton, Florida